

2022-10

On wave impact pressure variability

Raby, Alison

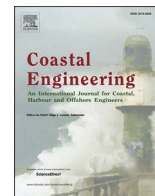
<http://hdl.handle.net/10026.1/19463>

10.1016/j.coastaleng.2022.104168

Coastal Engineering

Elsevier BV

All content in PEARL is protected by copyright law. Author manuscripts are made available in accordance with publisher policies. Please cite only the published version using the details provided on the item record or document. In the absence of an open licence (e.g. Creative Commons), permissions for further reuse of content should be sought from the publisher or author.



On wave impact pressure variability

Alison Raby^{a,*}, Geoffrey Bullock^a, Philip Jonathan^{b,c}, David Randell^d, Colin Whittaker^e

^a School of Engineering, Computing and Mathematics, University of Plymouth, Drake Circus, Plymouth, PL4 8AA, UK

^b Shell Research Limited, London, SE1 7NA, UK

^c UK and Department of Mathematics and Statistics, Lancaster University, LA1 4YF, UK

^d Shell Global Solutions BV, 1031 HW, Amsterdam, the Netherlands

^e Civil and Environmental Engineering, The University of Auckland, Auckland, 1010, New Zealand

ABSTRACT

The variability of the largest wave impacts, where nominally identical waves produce significantly different pressures, is widely known. However, the mechanisms are not well understood. Here we provide a review and investigation of factors affecting the variability of wave impact pressures on steep walls, quantifying the range of parameters that have been used in the literature. We then present two investigations: (i) Setup 1 on the effect of structure slope and (ii) Setup 2 on the effects of kinematics variability on pressure variability. Firstly, wave impacts arising from about 250 focused wave groups interacting with three values of wall steepness (vertical, 10° to the vertical, and 27° to the vertical) showed that steeper walls resulted in larger impact loads, the largest of which were experienced higher up the wall. The maximum pressure data was seen to be a good fit to the Gumbel model for the vertical wall but closer to the log-Normal distribution for the 10° wall. Parameter estimates for those distributions revealed a systematic variation which could potentially be used to predict maximum impact pressures at intermediate wall angles and locations. The pressure wave arising from the impact was seen to be of highly variable speed, for the 10° wall it was estimated to be about 10 m/s at the 1:25 model scale, decreasing for the 27° wall. In the second investigation, which provided kinematics data using particle tracking velocimetry, rapidly varying velocities close to the impact location were observed, with maximum values at impact being a reasonable fit to the Weibull distribution. Findings indicate that though the water surface may appear to be calm, residual sub-surface velocities undoubtedly play some role in the variability of the subsequent wave impact pressures.

1. Introduction

Humanity has long been aware of the destructive power of breaking waves and attempts to measure and characterise the resulting forces began when suitable instrumentation became available. Early advances were made by [Stevenson \(1886\)](#) and [De Rouville et al. \(1938\)](#) in the field and [Bagnold \(1939\)](#) in the laboratory, all of whom realised that breaking-wave impacts on a steep-fronted structure can generate very high pressures. Despite this, designers of structures required to withstand harsh coastal and offshore environments did not always fully appreciate the importance of wave-impact pressures, in part because the extreme pressures were thought to be too short-lived or localised to be of major significance. An analysis of breakwater failures carried out by [Oumeraci \(1994\)](#), in which breaking waves were blamed for the bodily displacement of massive caissons, did much to change this view and emphasised the need to take account of both the magnitude and duration of the associated forces ([Oumeraci et al., 2001](#)). Knowledge has also been gained concerning wave impacts' potential for causing localised damage to steep-fronted structures. Examples include the buckling of the bow plating on floating production storage and offloading (FPSO) systems such as those used by the oil industry in the North Sea ([Hodgson](#)

and [Barltrop, 2004](#)), and the propagation of impact pressures into cracks that can lead to the removal of blocks from masonry structures ([Bezuijjen et al., 2005](#)).

However, maximum wave impact pressures have been found to be highly variable for similar conditions, making their quantification prone to uncertainty. This aspect has received attention in a number of physical modelling investigations ([Bagnold, 1939](#); [Denny, 1951](#); [Hattori et al., 1994](#); [Bullock et al., 2007](#); [Cuomo et al., 2010a](#)). This paper reviews wave impact variability investigations to date, comparing some of the key parameters and statistical distributions used by investigators (Section 2). It then presents a sequence of two investigations, the first (Setup 1) designed to quantify the wave impact variability on three different geometries using large numbers of repeatable focused wave groups (Section 3) and the second (Setup 2), again using focused wave groups but extending the investigation to include the measurement of wave kinematics (Section 4). Concluding remarks are provided in Section 5.

* Corresponding author.

E-mail address: alison.raby@plymouth.ac.uk (A. Raby).

<https://doi.org/10.1016/j.coastaleng.2022.104168>

Received 1 October 2021; Received in revised form 4 May 2022; Accepted 23 June 2022

Available online 25 June 2022

0378-3839/© 2022 The Authors. Published by Elsevier B.V. This is an open access article under the CC BY license (<http://creativecommons.org/licenses/by/4.0/>).

2. Background

2.1. Causes of wave impact variability

Common to all wave impact tests is the fact that the maximum impact pressures vary substantially from one breaking event to another, even when the breakers originate from nominally identical waves. This is due to a variety of effects including the types of waves used, the 'noise' in the wave channel, i.e. residual motion from previous waves (Peregrine, 2003), and the turbulence due to wave breaking which can entrain or entrap air.

Several researchers have used regular wave trains (Mogridge and Jamieson 1980; Kirkgoz 1991; Hattori et al., 1994; Bullock et al., 2007), sometimes of just a few cycles because of the build-up of reflections in the channel (Marzeddu et al., 2017). However, even individual waves within a short regular wave train will be different due to the preceding waves modifying the next incident wave; in early tests by Mogridge and Jamieson (1980) it was estimated that wave height varied by $\pm 4\%$, though more recent tests by Marzeddu et al. (2017) on highly repeatable short duration regular waves interacting with a laboratory scale breakwater had a mean percentage error of 1% or less. Other researchers have used solitary waves: Bagnold (1939) reported that with a mains voltage fluctuation of the order of 3% it was not possible to control the wave such that there would be a succession of wave impacts. However, in the same lab some years later, Denny (1951) reported that a new control mechanism was devised to ensure repeatability of the paddle motion to within 2%.

Short wave packet or focused groups have been used by several investigators: small-scale deep-water tests were undertaken by Chan and Melville (1988) and full-scale tests for the SLOSH project in the Delta flume by Hofland et al. (2010). The latter tests revealed that flip-through impact types created largest variability. Reporting on the same project, but on both full-scale tests in the Delta flume and 1:6 'large-scale' tests in the Scheldt flume, Bogaert et al. (2010) calculated the coefficient of variation of various parameters, and confirmed that in the Scheldt flume, greatest variability in maximum pressures was seen for flip-through impacts (45%), then for impacts having trapped air pockets (15%), then sloshing impacts (0.1%), all for small numbers of tests (≤ 10). Furthermore, repeatability of tests in the Delta flume were affected by the wind (Hofland et al., 2010; Bogaert et al., 2010).

Wave impacts have also been simulated by dropping objects onto still water (e.g. Verhagen 1967; Zhu, 1995; Ma et al., 2016; Mai 2017). Mai (2017) found the repeatability of the drop test impact velocity was about 1–2% (standard deviation as a percentage of the mean) but the impact pressures varied by up to 9%. Battley and Allen (2012) reported differences of 3% in velocity and differences of 11.3%, 4.4% and 0.8% in the impulse at each of their transducer locations, for drop tests of a rigid panel at a nominal impact velocity of 5 m/s.

Finally, sloshing motion in fluid tanks is also known to give rise to significant impacts and has been the subject of much study in naval architecture and marine engineering (e.g. Faltinsen 1974; Akyildiz and Erdem Unal, 2006; Song et al., 2013). Song et al. (2013) used the Bubble Image Velocimetry to try to establish a relationship between the velocity of the flow and the resulting pressures in the tank. They used data from a single sloshing test cycle, and repeated the test 20 times. They do not provide a quantification of the repeatability of the motion, or the highest impact pressures, though they give a standard deviation of more than 20% for the maximum velocities.

In a bid to reduce the effect of residual motions, the flume should be allowed to settle for an appropriate time period between tests. Denny (1951) ran two sets of tests, firstly in 'calm' water (with a 15–20 min delay between wave trains) and 'disturbed' water (with no delay) and found that the average impact pressures were reduced by 50% if the water was disturbed (cited by Walkden and Bruce, 1999); Chan and Melville (1988) allowed 30 min between wave groups; Kirkgoz (1990) limited his tests to 20 waves after which he waited about an hour; Hull

and Muller (2002) allowed just 2 ½ minutes between tests that comprised 5 or 6 waves; and Marzeddu et al. (2017) waited 3 min (A. Marzeddu 2017; personal communication). Disturbances caused by preceding wave breaking were discussed by Bogaert et al. (2010); these necessitated the redesign of a series tests in the large Delta flume.

Furthermore, because impact pressure maxima are both spatially and temporally localised, the accuracy and repeatability of the measurements are affected by: the number and spacing of the sensors; and the data collection rate. To reduce the spatial limitations of their transducer array, Stagonas et al. (2016) used a pressure mapping system, which had 196 sensor elements uniformly distributed over a 71 mm \times 71 mm square. Currently this technology is not widely used because of challenges related to calibration, longevity and cost. Kimmoun et al. (2010) used a remarkable 88 pressure sensors, in a cruciform configuration but the repeatability of their experiments was negatively affected by issues such as variation in water depth due to evaporation. For reasons of economy and practicality, between five (Ma et al., 2016; Duong et al., 2019; Ha et al., 2020; Mai et al., 2020) and 15 (Song et al., 2013) sensors are normally used, with a bias towards the lower end, particularly in small-scale tests. Thus, the use of 6 sensors for the Setup 1 tests reported here, is in line with common practice in coastal engineering. Some investigations in maritime and naval applications have used much higher resolutions e.g., Chan and Melville (1988) who mention 29 transducer locations and Bogaert et al. (2010) who apparently had up to 300 locations. Certainly, higher resolutions would be desirable and could be obtained by positioning a limited number of sensors in different locations. However, this would be at the cost of a significant increase in repetitions, and with some uncertainty about whether extremes were captured for all configurations. Regarding the size of the sensor heads, for a large measurement area, the greater spatial averaging is likely to cause peak pressures to be underestimated but improve repeatability. Whilst peak pressures can be more accurately recorded by use of a transducer with a small measurement area, the chances of the head location coinciding with the peak are obviously reduced. As the impact location also varies, there is an unavoidable trade-off between resolution and repeatability. Furthermore, Kim et al. (2015) found size to be important from a sensitivity aspect, with a larger pressure transducer being more stable to changes of medium and temperature.

Debates around the acquisition rates necessary to accurately resolve the pressure time history have been running for some time. With the pressure spike lasting just a few tens of milliseconds it is necessary to acquire data in the range of kilohertz to get close to capturing the tip of the spike, otherwise the maximum impact pressure will be wrongly measured. The wide variety of acquisition frequencies that have been used in small scale experiments are shown in Fig. 1. Interestingly there is no clear trend of acquisition rates with time. Based on seminal wave loading experiments in the Large Wave Flume in Hannover, Schmidt et al. (1992) provided percentage loss results in maximum pressures, suggesting that a sample rate of 1 kHz may result in a 7% underestimate in maximum impact pressure with respect to values obtained at 11 kHz. Mogridge and Jamieson (1980) surmised that improvements in the quality of experiments has resulted in larger pressures being attained, however some of the largest pressures ever recorded (Bagnold, 1939) used the most rudimentary equipment. Given that Bagnold (1939) used analogue equipment and therefore had no quantisation errors, it could be argued that analogue equipment with an appropriate frequency response should be used.

Finally, recent investigations have begun to shed some light on the causes of the hydrodynamic variability. Lubin et al. (2019) and Dias and Ghidaglia (2018) suggest instabilities on the wave crest are the source of wave impact variability. van Meerkerk et al. (2021) investigate this effect using focused wave groups to generate a plunging breaking wave on a vertical wall, measuring gas flow dynamics around the wave crest tip, using planar particle image velocimetry and stereo planar laser induced fluorescence. Their experiments revealed the presence of vortices, and they conclude that the gas phase could affect the impact pressure

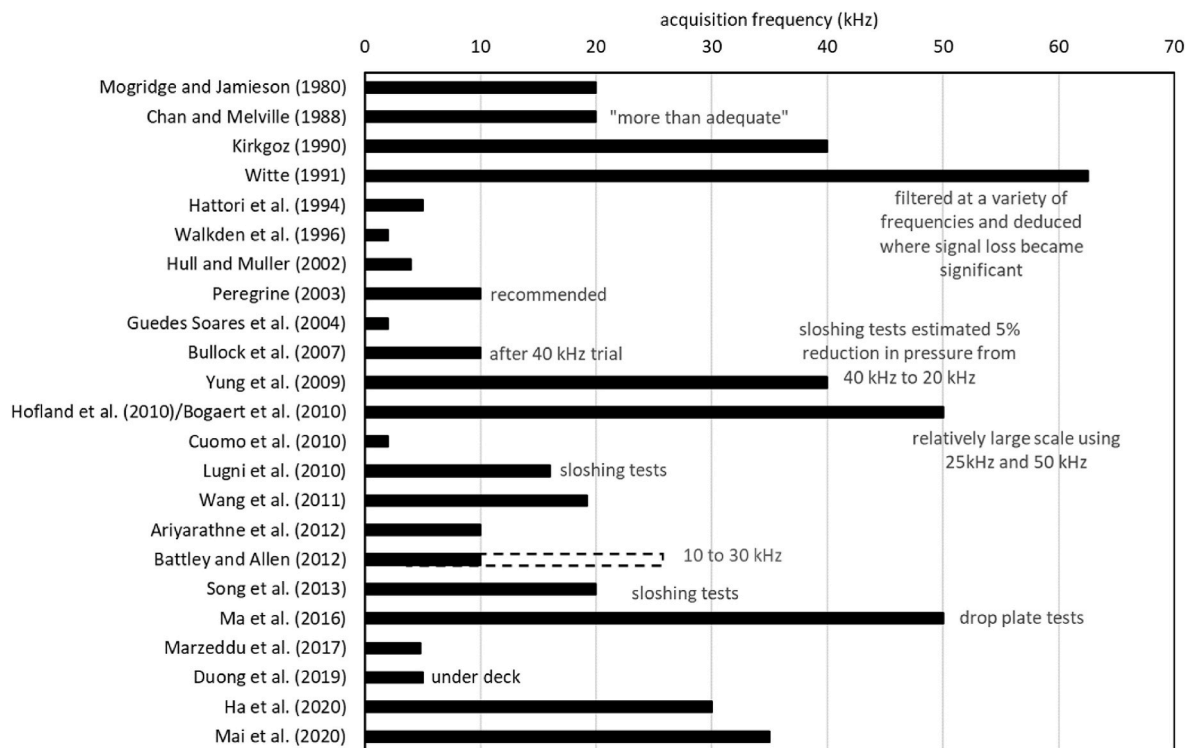


Fig. 1. Range of data acquisition frequencies used in laboratory wave impact tests (unless labelled as sloshing or drop plate tests) (Ariyaratne et al., 2012; Guedes Soares et al., 2004; Lugni et al., 2010; Wang et al., 2011; Yung et al., 2009).

variability, because it contributes to the variability of the impact location. van Meerkerk et al. (2021) also mention the effects of temperature variation and the presence of surface particles *i.e.* dust.

2.2. Quantification of the maximum impact pressure variability

Several investigators have attempted to quantify the variability of maximum pressures using regular waves: Walkden et al. (1996) presented the probability of occurrence of maximum pressures, but commented that the interpretation of such results for design purposes was not clear; Mogridge and Jamieson (1980) produced cumulative probability distributions for wave impact data from solid and perforated caisson walls; Hull and Muller (2002) presented scatter graphs showing the spread in maximum pressure measurements at different wave heights; and Bullock et al. (2007) provided percentage exceedance curves for four different impact types identified, which could be used to give an indication of wave impact severity.

The starting point for a theoretical approach to quantifying variability is the quantification of the level of air entrained or entrapped in the breaking wave that leads to random behaviour. Führböter (1987) postulated that the thickness of an air cushion at the structure (Bagnold, 1939) is strongly stochastic and follows a Gaussian distribution. In this case the maximum pressures, which are related to the size of the air cushion, can be fitted by a log-Normal distribution. This distribution was subsequently used by Witte (1991) and Kirkgoz (1990, 1991, 1995) to present their own data. However, the early PROVERBS (Probabilistic design tools for vertical breakwaters) project investigations (Kortenhaus, 1997; Oumeraci and Kortenhaus, 1997), which used data from a number of different tests (McConnell and Kortenhaus 1996; Kortenhaus et al., 1994; Allsop et al., 1996), considered several distributions. Kortenhaus' (1997) results showed that the log-Weibull distribution, with parameters estimated using linear regression, provided the best fit to breaking wave impact data. However, following further analysis by project partners, the final suggestion in the PROVERBS guidance (Oumeraci et al., 2001) was to use the General Extreme Value (GEV)

distribution; whilst there was limited difference in the fit, it was deemed to provide greater flexibility (A. Kortenhaus 2012; personal communication). Cuomo et al. (2010b) fitted wave impact and pressure rise time (time to achieve the maximum pressure) data from irregular wave tests to a joint-probability distribution which permits conditional and coupled occurrences to be deduced. Subsequently Marzeddu et al. (2017) used short-duration regular wave trains and proposed the gamma distribution for maximum pressures and the GEV for maximum forces.

The effect of wall angle on the maximum impact pressures and variability has been the subject of some investigation, but the findings are not consistent. Richert (1968) found that it was not possible to create the same size shock pressures on a wall inclined at 30° to the vertical compared with those on a vertical wall, due to no air cushion being entrapped. In contrast, Kirkgoz (1991) investigated walls inclined at several angles to the vertical (-5°, 0°, 5°, 10°, 20°, 30° and 45°) and found that the maximum impact pressures increased as the wall slope decreased from vertical to 30°, before the pressures then decreased on the 45° wall. A possible explanation for this apparent anomaly is that Kirkgoz optimised his waves to produce 'perfect breaking' on each wall slope, thereby changing the input characteristics as well as the wall slope. On the wave impact variability, Kirkgoz plotted maximum impact pressures on log-Normal graphs onto which data from the 0° and 10° walls collapsed. However, for the 30° wall the largest pressures showed a higher probability of occurrence than the normal distribution. Bullock et al. (2007) conducted tests at both 0° and 27° in the GWK but only provided percentage exceedance curves for the vertical wall. They mention that the loading (pressure, force and impulse) on the sloping wall tended to be less than on the vertical wall for the same wave cases, though there were fewer tests on the sloping wall.

These statistical treatments require large data sets to give confidence in the distributions; Davey et al. (2008) warn of the difficulties in fitting distributions at the extremes where data are scarce. Kortenhaus (1997) suggests that a minimum of 250 data points is required. Chan and Melville (1988) obtained a large number of wave impacts for different

breaking wave types, but for identical tests had a maximum of only 10 repeats. Mogridge and Jamieson (1980) had 300 tests but used sets of 10 regular waves so they were not strictly repeatable, as already mentioned. Marzeddu et al. (2017) experiments used 120 repeat tests for four different regular wave trains.

Exhibiting less variability and therefore of greater use in design guidance is the pressure- or force-impulse: the time-integral of pressure (or force). Both Denny (1951) and Walkden et al. (1996) present frequency distributions for maximum impact pressures and impulse, demonstrating that the impulse distribution is much more compact, i.e. less variable, than the pressure maxima, confirming the findings of others e.g. Chan and Melville (1988).

In conclusion, it has been established that to obtain the most repeatable wave impacts it is necessary to minimise residual motions, to allow the water to settle between tests, to sample data at a high enough rate to capture the peak value, to have a high spatial distribution of pressure sensors, and to have sufficient repeats for findings to be statistically significant. The following tests were designed to fulfil these requirements, excepting the high spatial distribution, as tests used a relatively modest number of conventional sensors. The tests methodically investigate the effect of wall slope on the variability (Setup 1) and relate the underlying kinematics to the resulting impact pressures (Setup 2).

3. Quantification of wave impact variability on different slopes

3.1. Experimental setup 1

Tests reported here were conducted as part of the Breaking Wave Impacts on COastal STRuctures (BWIMCOST) project (Bullock et al., 2007) and as such were undertaken on a 1:25 scale model of Admiralty Breakwater in Alderney, constructed in a 20 m wave flume (see Fig. 2) with a still water level (SWL) 750 mm above the flume bed and 200 mm above the toe of the wall. Three wall slopes were investigated: 27° to the vertical (similar to the Admiralty Breakwater), 10° to the vertical and a vertical wall.

In order to produce impacts with the highest degree of repeatability, and an appropriate representation of large ocean waves, focused wave groups were used (see also Chan and Melville, 1988; Hofland et al., 2010; Whittaker et al., 2016). In contrast to the work of Kirkgoz (1990, 1991, and 1995) who optimised his wave for each wall slope with a view to producing the maximum impact on the slope being used, in the current investigation the same focused wave group was used on all three wall slopes. This provides a more stringent test of the effect of identical offshore conditions on different wall geometries. Waves were generated with a wedge-type wavemaker (Bullock and Murton, 1989).

An optimisation process was initially undertaken to find the wave that produced the largest impact on the 27° wall, subject to the sample of tests used. This same wave produced some of the highest impact pressures on the vertical wall so was subsequently used on the vertical and the 10° wall. The simple input signal for a focused group is described by Hunt-Raby et al. (2011), but here we also included second order corrections (Barthel et al., 1983) plus those due to evanescent modes (T. Baldock 2004; personal communication, 15 May). The group had a Pierson-Moskowitz spectral shape, defined by 34 wave components

across a frequency band of 0.293 Hz–1.454 Hz, with a peak frequency of 0.5 Hz. It had a nominal central crest amplitude of 390 mm and a target focus location 11 m from the paddle. Preliminary tests were conducted to determine how long the water would take to settle between runs; 10 min was deemed sufficient for this compact wave packet.

Surface elevation time histories were obtained using resistance-type wave gauges placed at up to 13 locations, as stated in Table 1, with a data acquisition rate of 30 Hz. Data have been presented with time zero ($t = 0$ s) corresponding to the time of maximum force on the wall. A total of 99 data sets are available for both the vertical and 27° walls, and 46 sets for the 10° wall.

In order to determine impact pressures, six 10 mm diameter XPM10 FGP Sensors pressure transducers were placed along the vertical centreline of the wall at elevations shown in Table 1. Pressures were recorded at 10 kHz by means of a desktop computer containing a National Instruments logging card NI PCI-6013, 16-Bit, 16-Analogue-Input Multifunction DAQ, and National Instruments LabVIEW logging software. Synchronisation between wave gauge and pressure transducers was achieved by including a 5 V trigger pulse in the surface elevation measurements as the pressure data acquisition commenced. However, the 33.33 ms duration between surface elevation data points was found to be insufficient resolution to precisely synchronise the impact pressure peaks between tests. Therefore a further level of synchronisation was undertaken, using a least-squares fit to the preceding quasi-hydrostatic signal that arose from a highly repeatable gentle sloshing wave. Force time histories were estimated by linear spatial integrations of the instantaneous pressures over areas as shown in Fig. 3, on the assumptions that a) the pressure measured by each transducer was constant up to the mid-point between adjacent transducers; b) the pressure measured by P1 remained constant below P1 for half the vertical distance between P1 and P2 and c) the pressure measured by P6 remained constant above P6 for half the vertical distance between P5 and P6.

3.2. Surface elevation variability

Fig. 4 (a) shows mean surface elevations for WG1-WG13 as the wave

Table 1
Setup 1 wave gauge and pressure transducer locations.

Wave gauge ID	Gauge location offshore of the wall toe (m)	Pressure transducer ID	Transducer location above SWL (mm)		
			Vertical wall	10° wall	27° wall
WG1	5.025	P1	2	2	2
WG2	3.765	P2	46	45	40
WG3	3.130	P3	78	77	68
WG4	2.785	P4	123	121	108
WG5	2.650	P5	163	161	143
WG6	1.125	P6	208	205	183
WG7	0.925				
WG8	0.720				
WG9	0.525				
WG10	0.320				
WG11	0.230				
WG12	0.123				
WG13	0.025				

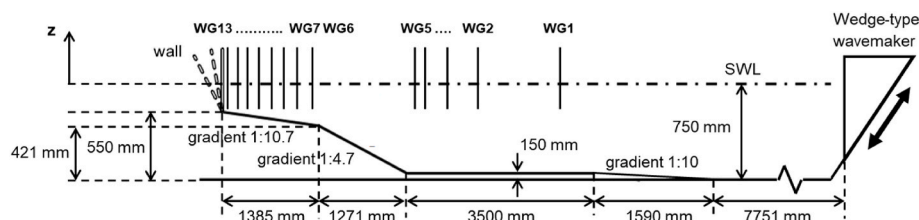


Fig. 2. Schematic diagram of Setup 1 wave flume, indicating approximate wave gauge (WG) locations and details of the bathymetry (not to scale).

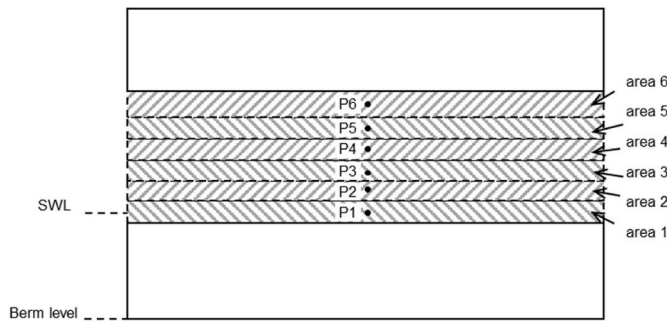


Fig. 3. Schematic diagram of wall showing pressure transducer locations and the respective areas over which forces were determined.

group propagated along the channel to the vertical wall. The position of WG4 corresponds to the apparent focus location of the wave group when the troughs either side of the central crest are the same size. This location is 1.7 m shoreward of the specified focus location but this discrepancy is to be expected due to nonlinear interactions between wave components (Baldock et al., 1996). The measured central crest amplitude at WG4 was of the order of 160 mm, far smaller than the nominal amplitude of 390 mm; it is likely that a manual adjustment was made to the generator gain, to reduce the size of the focused group to avoid wave breaking far from the wall. WG11 - 13 suffered from signal drop-out from the trough as they were situated in very shallow water. There was also electrical interference due to their close proximity to the bed, so they are not used in further analysis.

Data from 99 overlaid tests are shown in Fig. 4(b)–(g). They show a high degree of repeatability before the impact, but less so afterwards. There is also a discernible reduction in repeatability for gauges closer to the wall, particularly for WG8 and WG10. The root mean square error of the impacting wave surface elevation (determined from preceding trough to subsequent crest) as measured at the closest wave gauge to the paddle (WG1), is 3.0%. This compares reasonably well to the highly repeatable tests of Marzeddu et al. (2017), who achieved 1.3% for their linear wave and 2.9% for their cnoidal wave, both determined at a distance of 3 m from their paddle. One source of the relatively high error is that surface elevation data were acquired at 30 Hz, compared to 100

Hz by Marzeddu et al. (2017). N.B. WG6 – WG13 data were only acquired for the vertical wall investigations due to the considerable time taken for daily calibration of the gauges and the limited additional information that they provided. Note also from Fig. 4 (a) that the wave gauges closest to the wall (WG11 – WG13) show clipping of the signals, but these data are not used for any subsequent analysis.

3.3. Pressure variability

Fig. 5 shows pressure time history data from 99 repeat tests on the vertical wall at the lowest pressure transducer, P1, where blue dots indicate individual data points. The mean curve, indicated by the solid black line, shows the typical ‘church steeple’ shape characteristic of wave impacts (Peregrine, 2003). The time variable, t' , is with respect to the time of the mean curve peak. A good degree of repeatability is evident just before the impact and during the smoothly varying

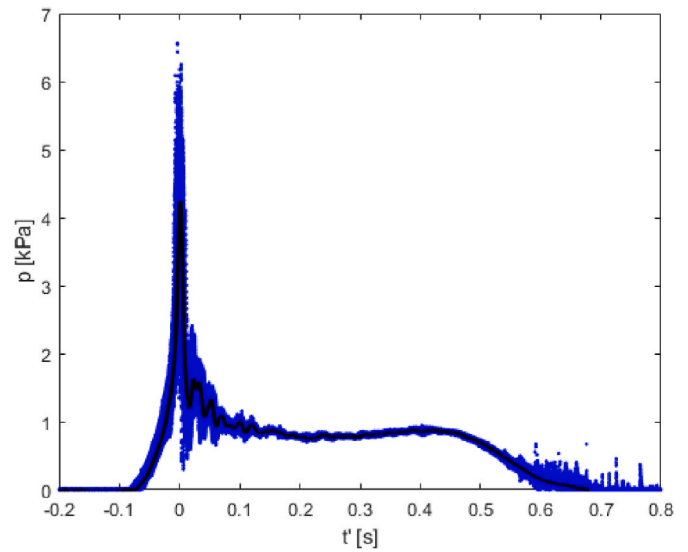


Fig. 5. 99 repeated pressure time histories at P1 on the vertical wall: Blue dots indicate data acquired at 10 kHz and the black solid line is the calculated mean.

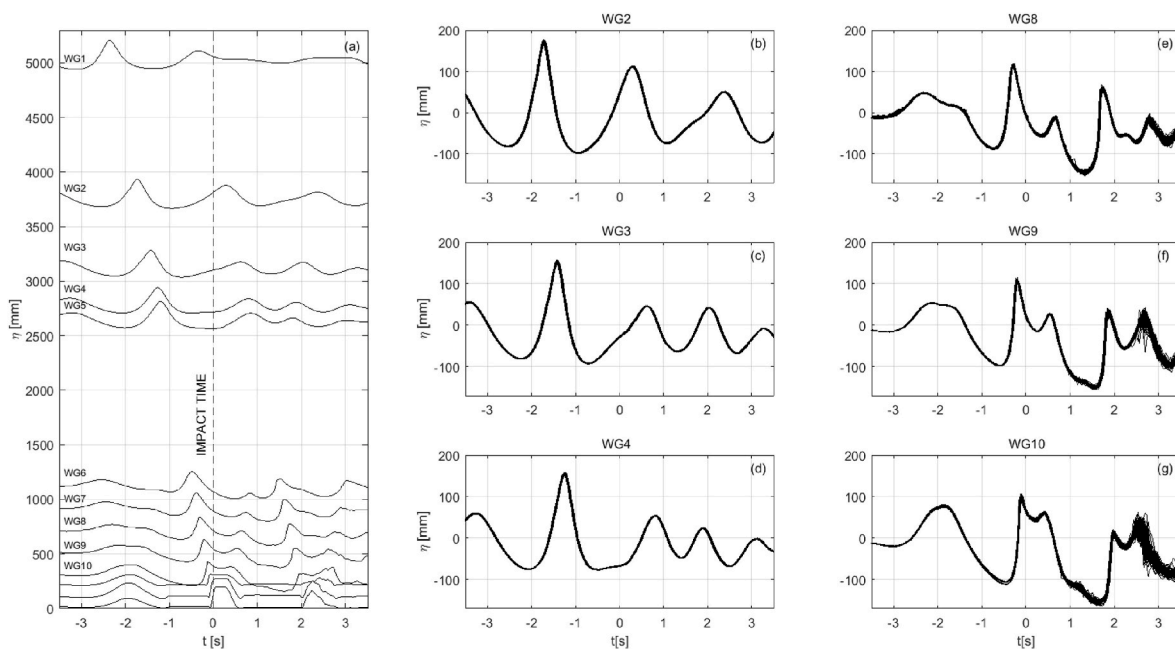


Fig. 4. Vertical wall surface elevation time histories (a) mean measurements at the gauge locations and (b) to (g) 99 overlaid tests from six selected wave gauges.

pseudo-hydrostatic region between 0.2 s and 0.5 s after impact. Beyond 0.5 s the data become more variable again, which may be due to spray falling back onto the water surface. The oscillations after impact indicate that most, if not all, of the impacts were of the high-aeration type (Bullock et al., 2007); the scatter of results suggests that the amplitude of the oscillations varied from test to test. If the frequency of the oscillations also changed, it would suggest that there was significant variation in the volume of air trapped (Minnaert, 1933; Hattori et al., 1994), but that has not been investigated here.

Coefficients of variation of the maximum impact pressures at each of the transducer locations varied from 8% to 103% (Table A1, Appendix A), higher than those reported by Bogaert et al. (2010) (0.1% for sloshing wave, 15% for an air pocket and 45% for flip-through type impact). This difference may be due to the lower resolution of pressure gauges in the present tests.

3.4. Pressure and force frequency distributions

Fig. 6 presents maximum pressure and horizontal force empirical densities for the three wall slopes. In terms of wall slope, the ordering of empirical densities for maximum pressure and force is the same. It can also be seen that the densities for maximum force are somewhat more separated than those of maximum pressure. Finally, the densities for maximum pressure, especially at 10° deg and 27°, exhibit longer right-hand tails. Summary statistics are provided in Table B1 (Appendix B). These show that the relative standard deviation (standard deviation/mean) of both the maximum pressures and forces generally decreases with increasing wall steepness.

3.5. Spatial distributions of pressures

In order to understand the spatial evolution of the wave impact, Fig. 7 presents pressure data at elevations (z) with respect to SWL at five instances in time, for the three walls, indicating the extent of the impact zone. The first observation is that the highest pressures occur some distance above the SWL. Different locations of maximum impact pressure have been reported in the literature, with Hull and Muller (2002) suggesting that the position is likely to be dependent on wave shape at impact. Hofland et al. (2010), who used focused wave groups, also report maximum impact pressures above SWL. Secondly, the elevation of the maximum pressures seems to increase with increasing wall steepness: on the vertical wall the maximum pressure recorded during an experiment only ever occurred at transducers P4 and P5; on the 10° wall maximum pressures also occur at around P4 to P5; and on the 27°

wall maximum pressures are lower down, at transducers P2 to P3. Kirkgoz (1995) also found that the maximum point of the distribution curve became progressively lower for less steep walls. However, he discovered that the location of maximum pressures showed a much larger variability than is evident from the current data. Thirdly, looking at the mean values at $t = 0$ s, the impact pressure is generally reduced for gentler slopes. But defying this trend, the highest impact pressure recorded at $t = 0$ s occurred on the 27° wall; this anomalous result is likely to be due to the optimisation of wave impacts for this wall geometry.

3.6. Pressure probability distributions

Illustrations of the fits of Weibull, Log-Normal and Gumbel distributions to the empirical distribution of maximum pressure measurements at each location P1, P2, ..., P6 and wall angle 0°, 10° and 27° are given in Fig. 8. The probability density functions for the three distributions are as follows.

Weibull:

$$f(x|\lambda, k) = \frac{k}{\lambda} \left(\frac{x}{\lambda}\right)^{k-1} e^{-\left(\frac{x}{\lambda}\right)^k} \quad (1)$$

where variable $x > 0$ represents maximum pressure here, and $\lambda > 0$ and $k > 0$ are scale and shape respectively;

log-Normal:

$$f(x|\mu, \sigma) = \frac{1}{x\sigma\sqrt{2\pi}} \exp\left\{-\frac{(\ln x - \mu)^2}{2\sigma^2}\right\}, \quad (2)$$

where μ is the mean and $\sigma > 0$ is the standard deviation; and.

Gumbel:

$$f(x|\mu, \beta) = \frac{1}{\beta} \exp(-z + e^{-z}), \quad (3)$$

where $z = \frac{x-\mu}{\beta}$, for location μ and scale $\beta > 0$.

In general, all model forms give a reasonably satisfactory description of the empirical distribution of measurements. For quantitative comparison of the different models, Table 2 gives corresponding Kullback-Leibler (KL) divergences. The KL divergence is a measure of the difference between two distributions; a value of KL divergence of zero indicates perfect agreement between the distributions, with quality of agreement decreasing with increasing value of KL divergence. For each

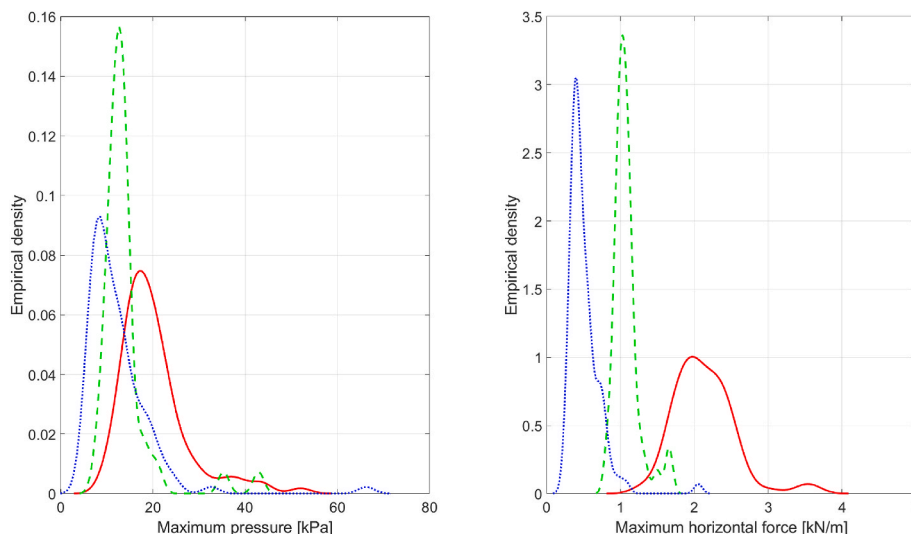


Fig. 6. Empirical densities of (a) maximum recorded pressures and (b) maximum estimated forces: red _ 0°; green - - 10°; blue ...27°.

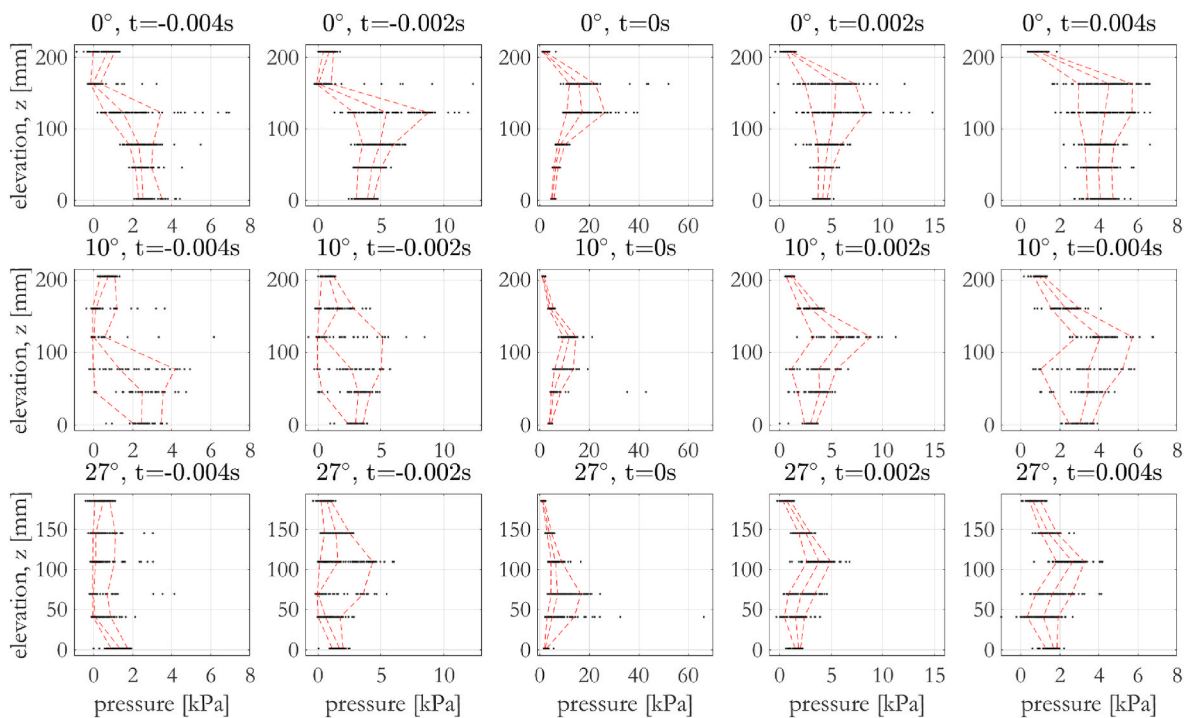


Fig. 7. Vertical spatial distribution of maximum impact pressure at elevations above the SWL at five instances in time (sequential columns) for each wall slope (sequential rows): dots indicate individual maxima and dashed red lines indicate the 10, 50 and 90 percentile values.

combination of location and angle, the minimum KL divergence over the Weibull, Log-Normal and Gumbel models is given in bold for convenience in Table 2.

No single model form gives best performance overall, with the Weibull model performing more poorly, with lower KL divergence than the Log-Normal and Gumbel; the Weibull fit for 27° at location P1 is particularly poor. For location P6, e.g., the Gumbel model has in general the lowest KL divergence for all angles; yet at P4, the Log-Normal model is best for all angles. For angle 0°, the Gumbel model has in general the lowest KL divergence at all but one location (which happens to be the location of highest impact pressure), yet the Log-Normal model is to be preferred for most locations at angle 10°. Some very large pressure measurements were recorded at P2 and 10°, resulting in the best fit in terms of KL divergence for a Weibull model with long tail.

The corresponding parameter estimates from the Weibull, Log-Normal and Gumbel model fits as a function of location and angle are given in Fig. 9. There is some evidence of systematic variation of model parameter estimates with location and angle e.g., for the vertical wall (0°), the parameter \hat{a} steadily increases with elevation above the SWL, and the elevation associated with this peak reduces with increasing angle. Trends in the parameter \hat{b} are a little less clear, but for example estimates of its value gradually decrease with elevation for the vertical wall Weibull distribution, though they steadily increase for the same geometry for the Log-Normal distribution. Based on the trends it might be feasible to estimate a predictive model for maximum pressure at intermediate locations and wall angles. The parameter estimates in Fig. 9 are provided in Table C.1 of Appendix C, and can be used with the appropriate model form from equations (1)-(3), to provide a first estimate of the distribution of maximum pressure.

3.7. Pressure wave variability

To provide quantitative information about the characteristics of the pressure wave, we present the pressure wave celerity. This is estimated from the distance between adjacent sensors divided by the time that the pressure wave takes to travel between the adjacent sensors when the

pressure first exceeds a particular threshold, in this case 25% of the maximum pressure at a location. Positive velocities mean that the pressure wave goes up the wall, and negative means the wave is travelling down. Fig. 10 presents these results, which include 75% uncertainty bounds. Clearly there is a high degree of scatter in velocities for the lower locations, and on the vertical wall there are limited useful data over the entire extent of the transducers. The fact that scatter is so significant for the vertical wall compared to the sloping ones suggests that the nature of the pressure wave is more chaotic, likely being affected by air entrainment/entrapment. The celerity of a pressure wave is highly sensitive to the level of aeration, a void fraction of just 2% reducing it from 1450 m/s in pure water to about 85 m/s at atmospheric pressure (Bredmose et al., 2009). Whilst the ambient level of aeration in the still water in front of the focused-wave group will be much less than this, there is evidence (Bullock et al., 2001; Blenkinsopp and Chaplin, 2011) to suggest that, even in small-scale freshwater tests, wave breaking can temporarily increase the level of aeration to above 2%. ‘Infinite’ velocities were also obtained for some impacts where the pressure wave was experienced simultaneously at two transducers (within the limits of the data acquisition frequency, at least). For the 10° wall where there is greater confidence in the data at upper transducers, the data suggest that a pressure wave travels towards the top of the wall at a velocity not exceeding 10 m/s. The general behaviour towards the SWL is that the pressure wave travels downwards at very large negative velocities of the order of tens of m/s. The trend is similar for the 27° wall with upward moving velocities of slightly smaller values than for the 10° wall, presumably because the impact is less violent, and much smaller uncertainty bands at all locations except between the two lowest transducers. It should be noted that results might be affected by other causes such as the break-up of a crest which impacts two pressure sensors in close succession.

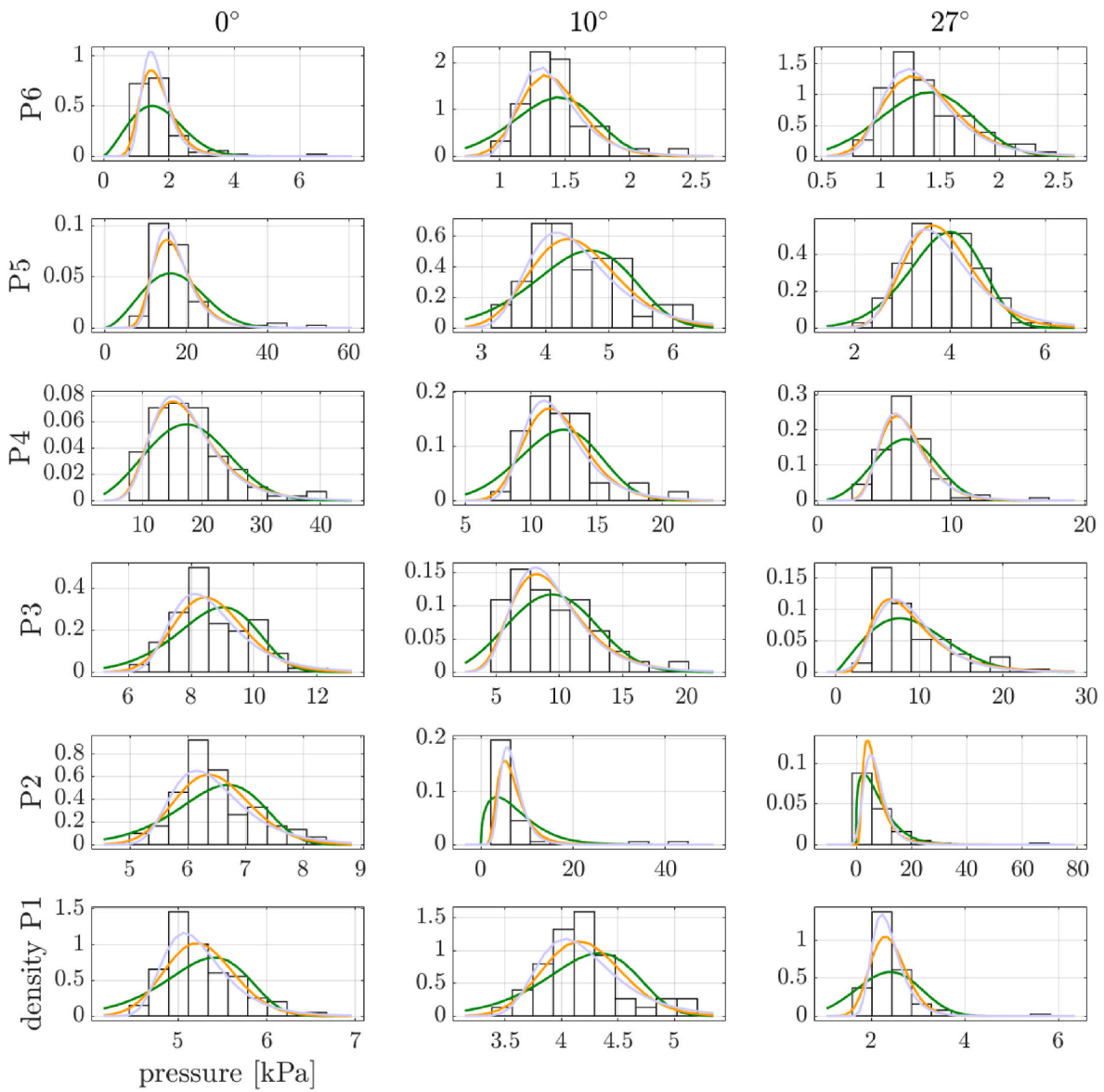


Fig. 8. Empirical densities (black) for maximum pressure at locations P1, P2, ..., P6 and angles 0°, 10° and 27° with corresponding Weibull (Wbl, green), Log-Normal (LgN, orange) and Gumbel (Gmb, blue-grey) fits.

Table 2

Kullback-Leibler (KL) divergences for Weibull (Wbl), Log-Normal (LgN) and Gumbel (Gmb) fits to the empirical distributions of maximum pressure values at 6 locations P1,P2, ..., P6 and three angles 0°, 10° and 27°. Values in bold are the minimum KL divergence for a given combination of angle and location. Perfect agreement corresponds to a KL divergence of zero.

	Wbl	P1	P2	P3	P4	P5	P6
0°		0.0473	0.0415	0.0372	0.0292	0.0787	0.0914
10°		0.0262	0.0428	0.0230	0.0184	0.0227	0.0310
27°		0.1123	0.0630	0.0403	0.0477	0.0258	0.0376
LgN							
0°		0.0311	0.0291	0.0298	0.0244	0.0359	0.0375
10°		0.0184	0.0506	0.0164	0.0150	0.0180	0.0199
27°		0.0362	0.0356	0.0338	0.0294	0.0258	0.0278
Gmb							
0°		0.0240	0.0279	0.0287	0.0288	0.0288	0.0374
10°		0.0207	0.0630	0.0165	0.0168	0.0146	0.0190
27°		0.0261	0.0536	0.0379	0.0316	0.0331	0.0245

4. Comparisons of kinematics and pressure variability

4.1. Experimental setup 2

The second set of tests were conducted on a vertical wall in a 20 m wave flume in the COAST Laboratory at the University of Plymouth, with bathymetry as indicated in Fig. 11. The SWL was set at 500 mm over the channel bed and 99 mm over the berm. Focused wave groups were again used, based upon a Pierson-Moskowitz spectrum with peak frequency of 0.464 Hz, and a theoretical crest amplitude of 100 mm with a measured wave amplitude of 104 mm at wg1. They had a theoretical focus location of 15.5 m, which places it 2.06 m beyond the wall. Preliminary corrections to second-order error waves were implemented in a similar manner to Whittaker et al. (2017), but with only partial success. The use of an apparently non-real focus location is merely a convenient way to control the relative phasing of the wave group properties (Whittaker et al., 2017), and was used here to produce wave breaking at the vertical wall. A number of repeat tests were conducted, 10 min apart, of which 10 tests were used in the data analysis. Resistance wave gauges with an acquisition rate of 128 Hz were positioned at locations shown in

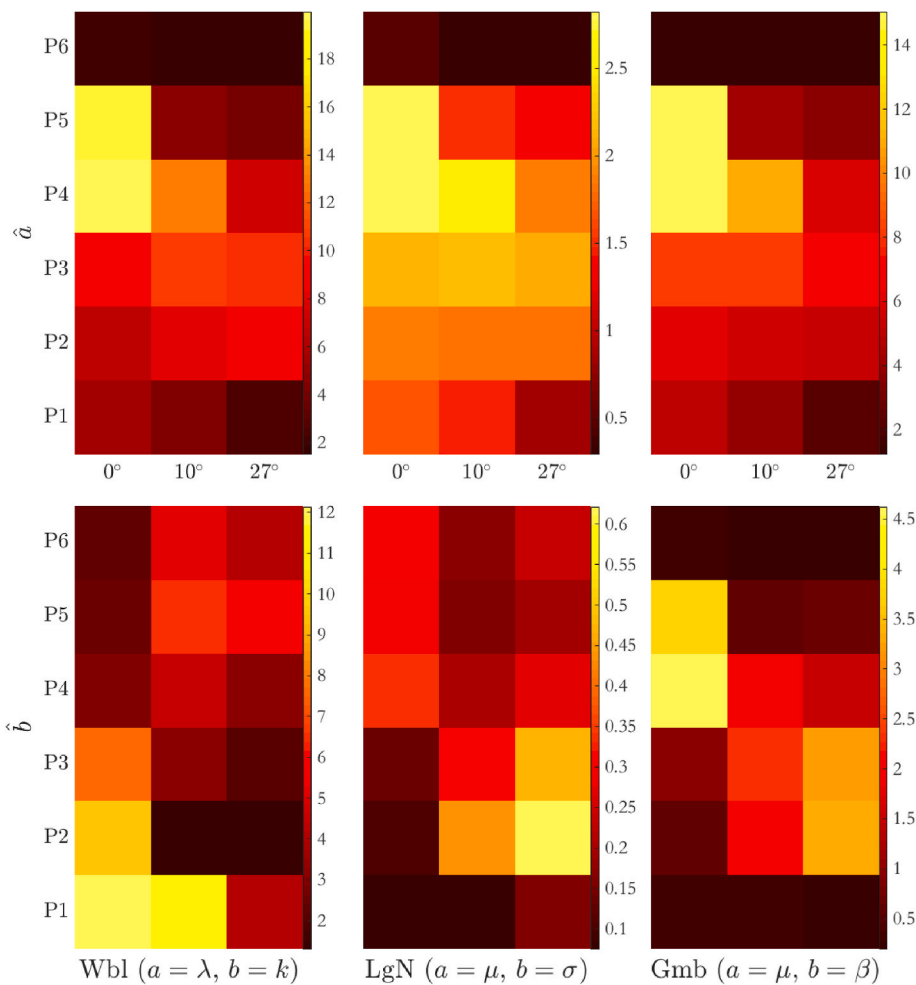


Fig. 9. Parameter estimates \hat{a} and \hat{b} for fits of Weibull (Wbl), Log-Normal (LgN) and Gumbel (Gmb) models to the empirical distribution of maximum pressure measurements for each combination of location P1, P2, ..., P6 and angle 0°, 10° and 27°. Referring to the equations in Section 3.6, the interpretation of parameters is as follows. For Wbl, $a = \lambda$, $b = k$; for LgN, $a = \mu$, $b = \sigma$; and for Gmb, $a = \mu$, $b = \beta$.

Table 3. Wave impact pressures were measured with a single FGP XPM10 sensor at 10 kHz, on the centre-line of a vertical wall, 202 mm above the berm which corresponds to 103 mm above the SWL.

Kinematics over the berm were determined using the particle tracking velocimetry (PTV) method (Nokes, 2021). A light box comprising a number of light-emitting diodes (LEDs) located above the flume illuminated fluid within a vertical (x,y) plane (see Fig. 11); this plane was located near the flume sidewall, offset from the wave gauge locations in the vicinity of the wall. The fluid was seeded with near-neutrally buoyant ‘Plascoat’ particles, approximately 150 μm in diameter, and a Photron SA4 high-speed camera located outside of the flume captured images of these illuminated particles during the impact process. The camera captured images at 125 frames/s, with a resolution of 1024 by 1024 pixels and a shutter speed of 1/200 s. The average number of particles per image was 2700, while the seeded water took an average of 40% of the total image area. With reference to the velocity field shown in Fig. 14, this yielded an average of 12 particles per grid point.

The PTV method involves processing the recorded images to identify and subsequently match particles between frames using an optimisation algorithm, providing the particle-centred displacements and velocities for the experiment. Applications involving tracking orbital particle motions under regular and focused wave groups (e.g. Grue and Kolaas, 2017; van den Bremer et al., 2019) directly use these Lagrangian measurements. To determine the Eulerian velocity field, these particle-centred velocities are subsequently interpolated onto a

rectangular grid using Thiessen Triangulation (see Nokes, 2021, for details). Obtaining robust Eulerian velocity fields may be challenging even in steady flows (e.g. Crowe et al., 2016), as the particle seeding density may limit the ability to resolve motions on small spatial scales (Nikora et al., 2007) and affect the overall repeatability of the experiments (Qiao et al., 2016). Unsteady phenomena such as focused wave group interactions with a vertical wall are further complicated by the significant spatial temporal variations in particle motion (complicating both the particle identification and tracking processes). Interpolation of particle-centred velocities can also cause issues in locations of significant free surface curvature observed in wave overturning during the breaking process, where velocities may be determined for grid points located above the free surface. The aeration introduced by wave breaking also renders particle identification impossible; Na et al. (2020) combined particle image velocimetry (PIV), bubble image velocimetry (BIV) and fibre optic reflectometry (FOR) to measure the flow structure and aeration under spilling breakers in the laboratory. Although the void fraction and post-breaking (i.e. following contact with the wall) velocity field are out of the scope of the present study, their findings regarding the need for a large number of repeat experiments are also relevant here. Reliable velocity data were obtained from 10 of 26 experiments, mostly due to challenges in identifying the rapidly moving particles prior to the impact upon the wall. In the following discussion, we focus our attention on the velocity measurements from grid points the locations indicated by red crosses A - F in Fig. 11.

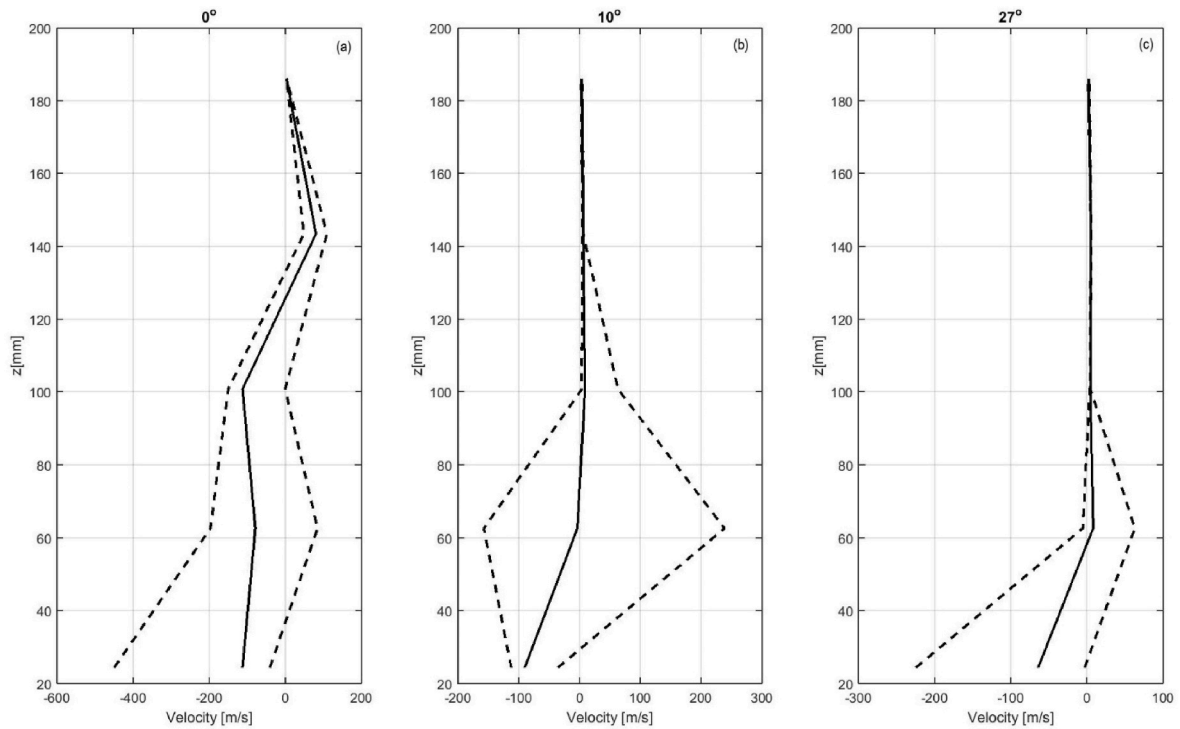


Fig. 10. Velocity of pressure wave from sensor to sensor at z elevations above with 75% uncertainty bounds.

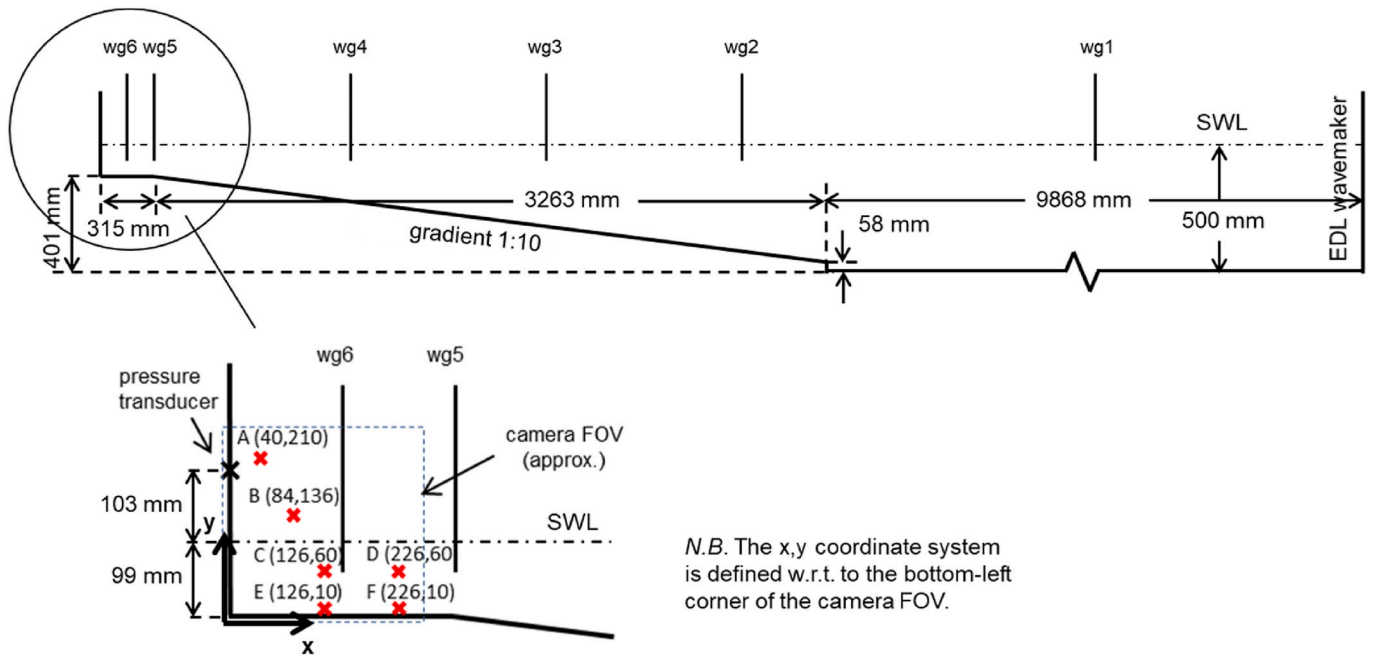


Fig. 11. Schematic diagram of Setup 2 indicating wave gauge (wg) locations and bathymetry, with an inset showing PTV locations (labelled A-F in mm with respect to the toe of wall), pressure transducer location and camera field of view.

4.2. Surface elevation variability

In the same manner as for the Setup 1 tests, Fig. 12 (a) shows mean surface elevations for the six wave gauge locations. Data from 26 overlaid tests are shown in Fig. 12 (b)–(g). The repeat tests show exceptional repeatability before the impact. As a comparison to the tests in Setup 1, for the wave gauge closest to the paddle (wg1), the maximum root mean square error is 0.68% (previously 3.0%), which is also lower than Marzeddu et al. The more modern paddle for Setup 2 and the

increased sample rate go some way to explaining the improvement from the Setup 1 results.

4.3. Pressure variability

Peak pressures were lower for the smaller wave in Setup 2, indicating a less violent impact. Correspondingly the coefficient of variation, c_v , was lower, at 26% (Table A2, Appendix A). The variability from the 10 repeats was investigated by plotting against a variety of probability

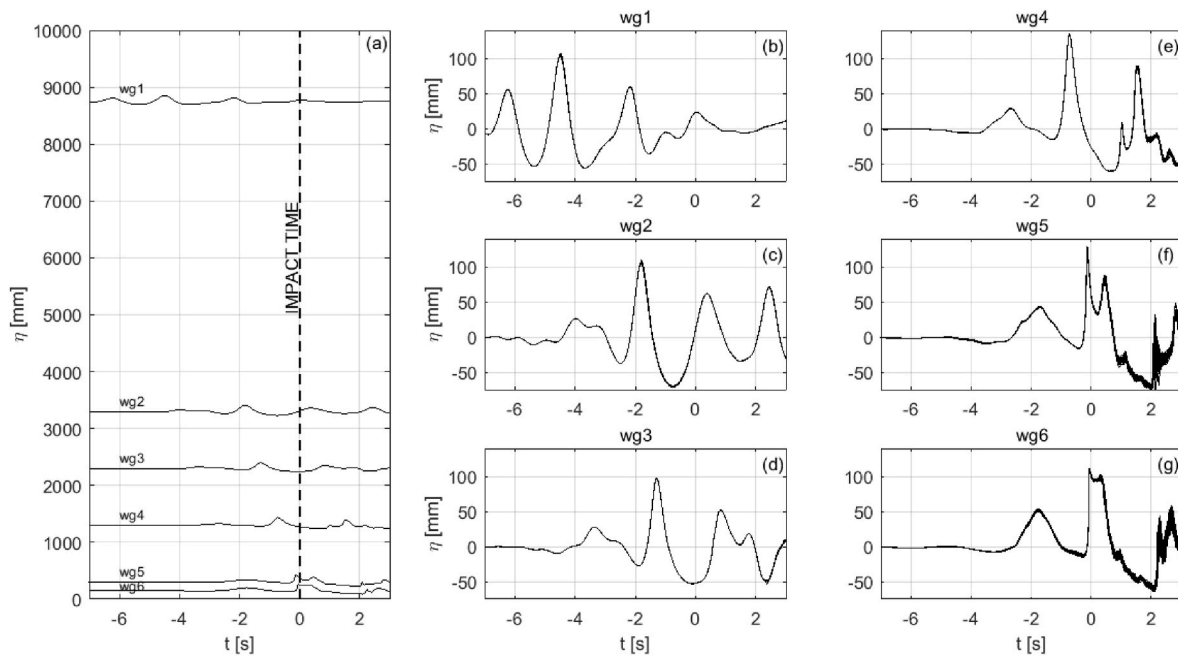


Fig. 12. Surface elevation time histories (a) mean values at the gauge locations and (b) to (g) 26 overlaid tests from each of the wave gauges.

Table 3
Setup 2 wave gauge locations.

Wave gauge ID	Gauge location offshore of the wall toe (m)
wg1	8.75
wg2	3.30
wg3	2.30
wg4	1.30
wg5	0.3
wg6	0.15

distributions, as in Setup 1, with the log-Normal and Gumbel distributions being reasonable fits (Fig. 13). The highest maximum pressure (test no. 27) is a relatively poor fit to the theoretical line, being larger than would be expected for these distributions. *N.B.* The pressure values are modest compared with the experiments in Setup 1, possibly due to the different bathymetry and the determination of pressure at just one location which may not have been at the very centre of the impact. The relatively poor fit to the extreme casts into some doubt whether it is possible to have confidence that particular probability distributions can usefully be applied between different setups, as the largest values will be of most interest. This case-dependence might be the root cause of the lack of agreement of probability distributions between investigators.

4.4. Kinematics variability

Fig. 14 illustrates the wave kinematics during the impact process, with the wave approaching the wall from the right of the images. Fig. 14 (a) illustrates the initial drawback of the water, followed by velocities in the upwards vertical direction in Fig. 14 (b). As the wave crest approaches the wall in Fig. 14 (c), the magnitudes of the velocities increase significantly. Fig. 14 (d) shows the wave overturning and the trapping of an air pocket, with horizontal velocities dominant at the moment of impact. Fig. 14 (e) shows the upwards motion of the wave immediately after impinging on the wall, while Fig. 14 (f) shows a moment of near stagnation before the drawback of the wave. Although not shown in the figure, this rapid drawback led to a turbulent flow with relatively large velocities at the water surface but negligible velocity magnitudes throughout the lower water column. Some vectors are visible above the illuminated free surface, due to some particles on the free surface (out of

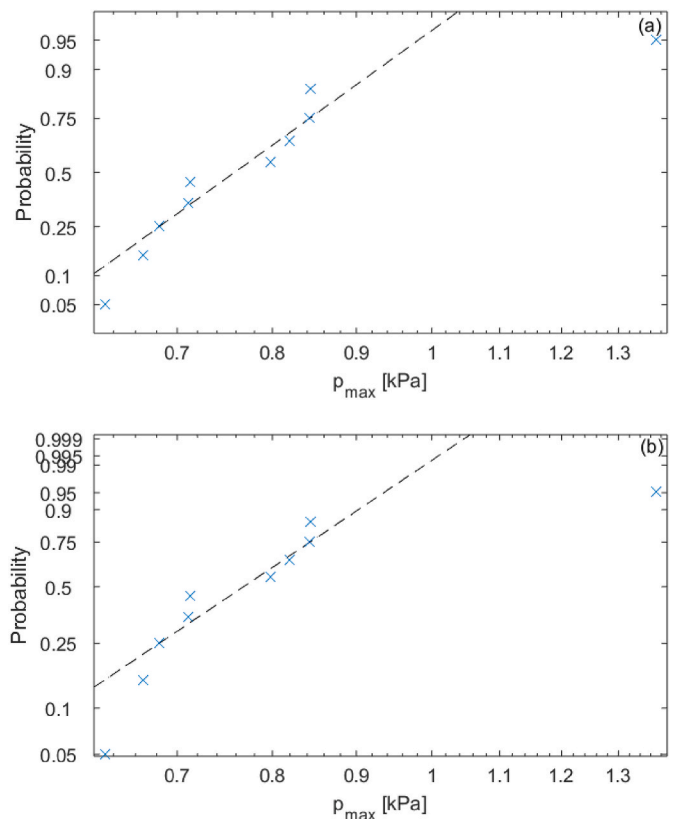


Fig. 13. Probability distributions for maximum impact pressures (a) Log-Normal and (b) Gumbel.

plane of the light sheet) or reflected from the flume sidewall being identified and tracked in the PTV algorithm, or the interpolation of particle-based velocities onto the rectangular grid in regions of significant free surface curvature (e.g. $t = -0.1$ s). However, these vectors were not used in any further analysis.

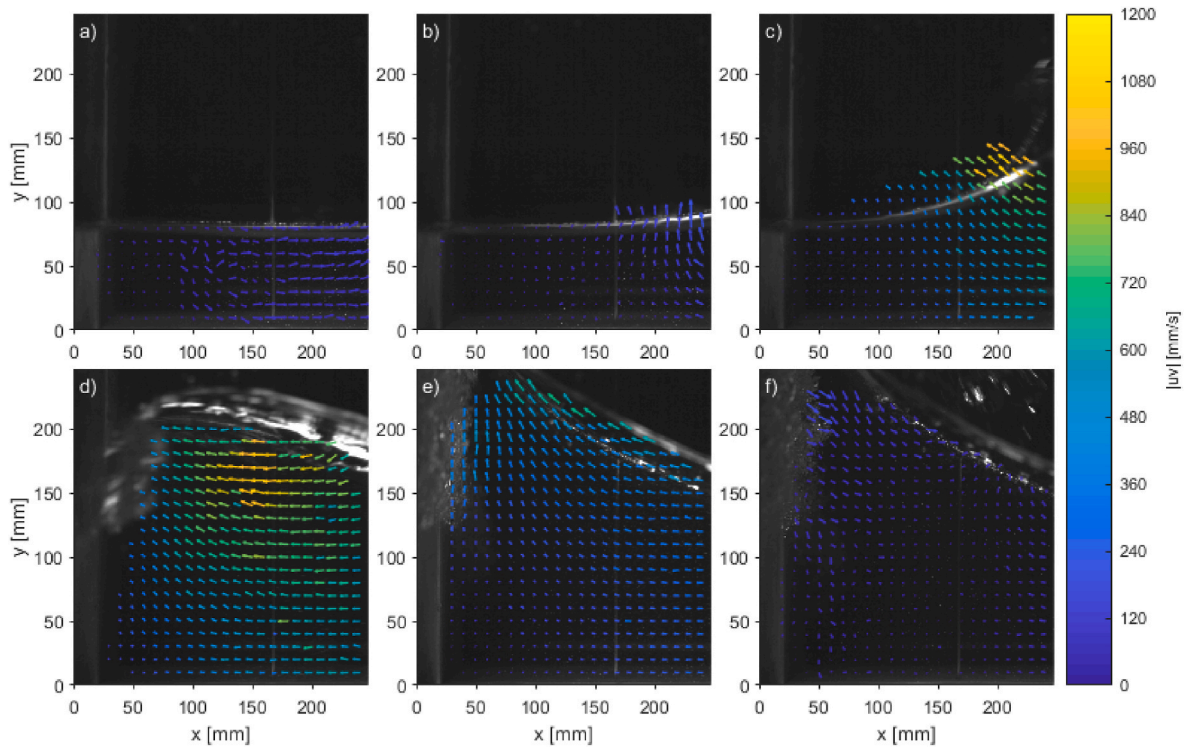


Fig. 14. Images and overlaid velocity vectors from the particle tracking velocimetry experiments recorded (a) $t = -0.3$ s, (b) $t = -0.2$ s, (c) $t = -0.1$ s, (d) $t = 0$ s, (e) $t = 0.1$ s, (f) $t = 0.2$ s, relative to the time of impact upon the wall. For ease of visualisation, the velocity vectors are normalised within each image to show the direction of the velocity field within the wave, while the colour scale represents the velocity magnitude.

Particle tracking velocity data from locations A to F (as shown in Fig. 11) are presented in Fig. 15 (a) to (f) respectively, overlaid with the surface elevation time history at the closest wave gauge to the wall (wg6). Positive velocities in the horizontal ($^{\circ}$) and vertical (\times) directions are towards the wall and vertically upwards, respectively.

Locations A and B are above the SWL so only have data for the time during which the wave travels over the berm and is then reflected back

from the wall. Velocity time histories at C–F (Fig. 15 (c), (d), (e) and (f) respectively) show very clear trends that correspond to the surface elevations on the berm: a fairly rapid increase to a maximum velocity (towards the wall) of 0.96 m/s at location D at the time of the maximum crest elevation, followed by a reversal of velocity to a maximum negative value (away from the wall) of about 0.59 m/s, again at D. The time of maximum positive velocity approaches $t = 0$ s, the closer the

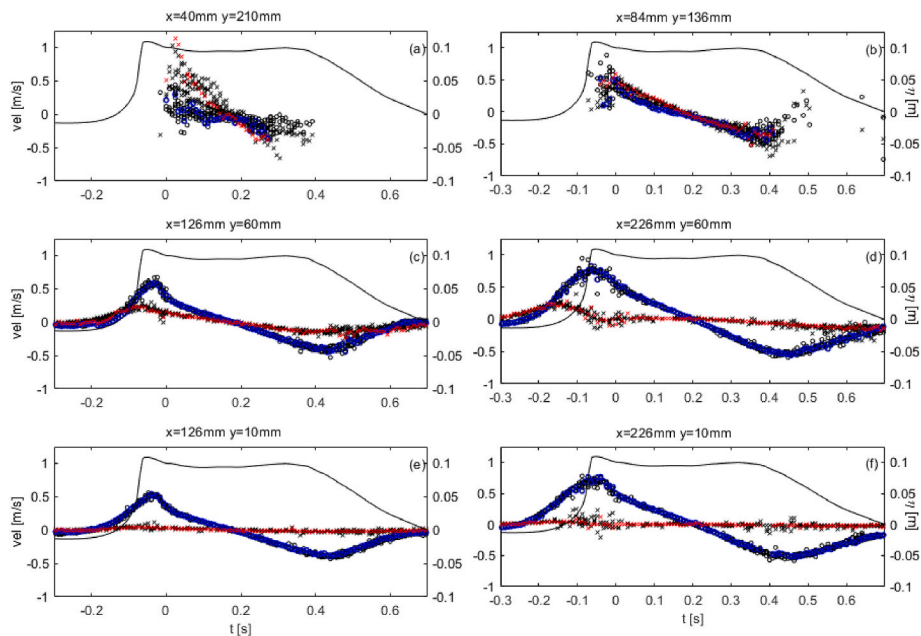


Fig. 15. Velocity and surface elevation time histories at locations A–F and wg6 respectively: $^{\circ}$ horizontal velocities, positive towards the paddle; \times (black) vertical velocities, positive upwards; $^{\circ}$ (blue) horizontal velocities for test no. 27, positive towards the paddle; \times (red) vertical velocities for test no. 27, positive upwards; solid line - surface elevation time history from wg6.

measurement location is to the point of impact, estimated to be about 215 mm above the wall toe.

The point of impact is defined as where the water in the leading edge of the overturning wave crest hits the wall. An alternative definition could be where an air pocket is trapped against the wall and compressed, as this can also cause high ‘impact’ pressures. However, this latter location would be slightly more arbitrary. The occurrence of the second (negative) maximum velocity follows a reduction in the local surface elevation as the reflected wave travels back down the flume. The velocity time histories at A and B follow the trends of the lower locations, except that the vertical velocities are greater than the horizontal ones, not unsurprising given the nature of the impact that sends water upwards as shown in Fig. 14 (e). The variability of the velocity data is greater around the time of impact and towards the impact location. Interestingly, the velocity data from test no. 27 were amongst the highest determined at locations A and B, providing some insight into why the measured pressure for that test was also the greatest. Finally, as shown in Table A3 (Appendix A), the coefficient of variation of the maximum absolute velocities, away from the impact area (locations C, D, E and F), are between 5% and 8%, whereas it rises substantially to 65% and 51% for locations A and B respectively, which are much closer to the impact area. These higher values are even higher than the c_v of the maximum measured impact pressures (26%).

Maximum horizontal velocities at location A, closest to the impact location, are shown to be a reasonable fit to the Weibull probability distribution as shown in Fig. 16. *N.B.* A negative data point has been omitted as the Matlab routine does not permit negative values.

5. Conclusions

This paper has reviewed factors affecting the variability of wave impact measurements on steep walls, describing the range of parameters that have been used in the literature. The review demonstrated the importance of minimising residual motions by allowing sufficient settling of water between tests, the requirement to sample at fast enough data rates to capture the peak pressure at a location (also requiring relatively high spatial resolution of sensors), and to have enough repeats for findings to be statistically significant. Two investigations were then described: in Setup 1 wave impacts arising from large numbers of focused wave groups interacting with three different wall steepness were presented. These repeatable wave groups, which generally caused high-aeration impacts, were used to show that the steeper the wall, the larger the impact load and the higher up the wall the maximum loads were experienced. Regarding probability distributions of the maximum pressures recorded at each location, the Gumbel model was most promising for the vertical wall at all but one location. However the Log-Normal model was a better fit for the 10° wall. Parameter estimates for the probability distributions suggest the presence of some systematic variations which could potentially be used for predicting pressure maxima at other locations and wall angles within the ranges tested here. This parameter-fitting approach might also form the foundation of a database of maximum wave impact pressures for a range of coastal structure configurations, analogous to the wave overtopping databases (EurOtop et al., 2018).

The pressure wave that was generated as a result of the impact was seen to be of highly variable speed, but for the 10° wall was estimated to be about 10 m/s at this laboratory scale, decreasing for the 27° wall. However, other phenomena such as impacts from the break-up of a crest, might also be responsible for these results. Sensitivity of all the variability findings to sensor spatial resolution would be worthy of further investigation. For Setup 2, a limited number of focused wave group repeats were undertaken, with the log-Normal and Gumbel distributions the best fit to peak pressures, but not being a good representation of the most extreme value. This suggests that probability distributions may be case-specific, perhaps explaining the variety of findings from investigators. Kinematics data available from a particle tracking technique

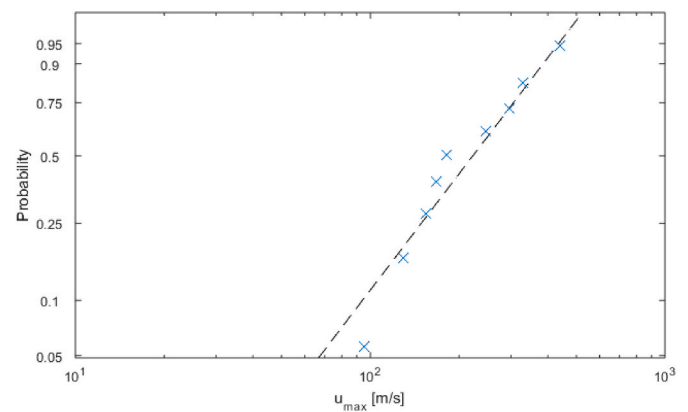


Fig. 16. Weibull probability distribution for maximum horizontal velocities at location A.

provided an insight into the flow close to the impact location, with maximum velocities being a fairly good fit to the Weibull distribution.

The high repeatability of the water surface elevation as measured by wave gauges in a modern laboratory wave facility, lulls us into a false sense of security. Clearly modern wave generators do not produce breaking waves with as repeatable flow/momentum flux fields as measurements of the variation of their water surface elevation lead us to expect. Recommendations arising from Setup 2 tests are to have: multiple pressure measurement locations to ensure that the pressure maxima are captured; faster video capture rates so that more precise comparisons between wave profiles could be made in both space and time; and more repetitions to obtain more statistically significant results. It would also be useful to use PTV techniques to investigate settling times between repeats, as it is undoubtedly the case that even though the water surface may be still, there is considerable water particle motion beneath the surface. These requirements are onerous but essential to truly accurately quantify wave impact variability. Considering the engineering application of these findings, the wave generation should also more closely model a real extreme *i.e.* NewWave, a design wave that comprises a small number of waves with a form that reflects the underlying statistical properties of a real sea-state and with an amplitude that has a meaningful exceedance probability (Whittaker et al., 2016; Vyzikas et al., 2018).

CRedit authorship contribution statement

Alison Raby: Conceptualization, Data curation, Formal analysis, Funding acquisition, Investigation, Methodology, Resources, Software, Visualization, Writing – original draft, Writing – review & editing. **Geoffrey Bullock:** Conceptualization, Funding acquisition, Investigation, Methodology, Project administration, Resources, Writing – review & editing. **Philip Jonathan:** Conceptualization, Data curation, Formal analysis, Investigation, Methodology, Software, Supervision, Visualization, Writing – original draft, Writing – review & editing. **David Randall:** Conceptualization, Data curation, Formal analysis, Investigation, Methodology, Software, Visualization. **Colin Whittaker:** Conceptualization, Data curation, Formal analysis, Investigation, Methodology, Supervision, Resources, Software, Validation, Visualization, Writing – original draft, Writing – review & editing.

Declaration of competing interest

The authors declare that they have no known competing financial interests or personal relationships that could have appeared to influence the work reported in this paper.

Acknowledgements

Setup 1 tests were undertaken as part of the UK EPSRC-funded

BWIMOST (Supplementary studies) project GR/T24708/01. We would like to thank the anonymous reviewers for their very helpful observations and suggestions.

Appendix A. Statistical properties of maximum impact pressures and velocities

Table A.1

Statistical properties (μ – mean, σ – standard deviation and c_v – coefficient of variation) of the maximum impact pressures from each of the Setup 1 tests.

	0° wall			10° wall			27° wall		
	μ [kPa]	σ [kPa]	c_v [%]	μ [kPa]	σ [kPa]	c_v [%]	μ [kPa]	σ [kPa]	c_v [%]
P1	5.3	0.40	8	4.2	0.36	9	2.4	0.47	20
P2	6.5	0.67	10	7.4	7.03	95	7.7	7.90	103
P3	8.7	1.16	13	9.5	3.14	33	9.1	4.68	51
P4	17.8	6.29	35	12.1	2.58	21	6.6	1.93	29
P5	17.4	6.52	37	4.5	0.71	16	3.8	0.72	19
P6	1.7	0.72	43	1.4	0.25	18	1.4	0.34	25

Table A.2

Statistical properties (μ – mean, σ – standard deviation and c_v – coefficient of variation) of the maximum impact pressures from Setup 2 tests.

μ [kPa]	σ [kPa]	c_v [%]
2.4	0.47	20

Table A.3

Statistical properties (μ – mean, σ – standard deviation and c_v – coefficient of variation) of the maximum horizontal velocities from Setup 2 tests.

location (Fig. 10)	μ [mm/s]	σ [mm/s]	c_v [%]
A	202	133	65
B	489	247	51
C	593	31	5
D	777	32	4
E	516	40	8
F	715	31	4

N.B. The coefficient of variation is the ratio of the standard deviation to the mean.

Appendix B. Summary statistics of maximum pressure and horizontal force empirical densities

Table B.1

Summary statistics (mean, μ , and standard deviation, σ) of maximum pressure (p) and horizontal force (F) empirical densities

wall angle	p [kPa]			F [kN/m]		
	μ_p	σ_p	σ_p/μ_p	μ_F	σ_F	σ_F/μ_F
0°	20.2	7.46	0.37	2.13	0.407	0.19
10°	14.0	6.07	0.43	1.08	0.175	0.16
27°	12.3	7.44	0.61	0.51	0.228	0.45

Appendix C. Parameter estimates of the empirical distributions of maximum pressure measurements

Table C.1

Parameter estimates of the empirical distribution of maximum pressure measurements from the Weibull, Log-Normal and Gumbel model fits, as a function of location and angle

	wall angle	P1	P2	P3	P4	P5	P6
Weibull a	0°	5.45	6.77	9.19	19.96	19.48	1.9
	10°	4.37	8.24	10.61	13.16	4.82	1.52
	27°	2.59	8.46	10.39	7.31	4.14	1.51
Weibull b	0°	12.13	9.64	7.65	2.94	2.58	2.32
	10°	11.41	1.41	3.18	4.55	6.59	5.11
	27°	3.97	1.29	2.11	3.28	5.78	4.14
log-normal a	0°	1.66	1.86	2.15	2.82	2.81	0.47
	10°	1.43	1.84	2.2	2.47	1.49	0.33

(continued on next page)

Table C.1 (continued)

	wall angle	P1	P2	P3	P4	P5	P6
log-normal b	27°	0.86	1.8	2.1	1.85	1.33	0.29
	0°	0.07	0.1	0.13	0.33	0.29	0.3
	10°	0.08	0.44	0.32	0.2	0.16	0.17
Gumbel a	27°	0.16	0.62	0.47	0.27	0.19	0.23
	0°	5.07	6.15	8.12	15.04	15.03	1.45
	10°	4.04	5.67	8.1	10.96	4.18	1.3
Gumbel b	27°	2.23	5.3	7.11	5.78	3.49	1.22
	0°	0.31	0.56	0.99	4.62	3.8	0.35
	10°	0.31	2	2.34	2	0.59	0.19
	27°	0.27	3.32	3.19	1.49	0.69	0.26

References

- Akyildiz, H., Erdem Unal, N., 2006. Sloshing in a three-dimensional rectangular tank: numerical simulation and experimental validation. *Ocean Eng.* 33, 2135–2149.
- Allsop, N.W.H., Vicinanza, D., McKenna, 1996. Wave Forces on Vertical and Composite Breakwaters. Strategic Research Report. Hydraulic Research Wallingford, Wallingford, UK. SR 443.
- Ariyaratne, K., Chang, K.-A., Mercier, R., 2012. Green water impact pressure on a three-dimensional model structure. *Exp. Fluids* 53, 1879–1894.
- Bagnold, R.A., 1939. Interim report on wave-pressure research. *J. ICE* 12 (7), 202–226.
- Baldock, T.E., Swan, C., Taylor, P.H., 1996. A laboratory study of nonlinear surface waves on water. *Phil. Trans. Roy. Soc. Lond.* 354, 649–676.
- Barthel, V., Mansard, E.P.D., Sand, S.E., Vis, F.C., 1983. Group-bounded long waves in physical models. *Ocean Eng* 10, 261–294.
- Battley, M., Allen, T., 2012. Servo-hydraulic system for controlled velocity water impact of marine sandwich panels. *Exp. Mech.* 52 (1), 95–106.
- Bezuijen, A., Muller, G.U., Wolters, G., 2005. Failure mechanisms for blockwork breakwaters. In: Allsop, N.W.H. (Ed.), *Coastlines, Structures and Breakwaters 2005*. International Conference on Coastlines, Structures and Breakwaters. Thomas Telford, pp. 121–131.
- Blenkinsopp, C.E., Chaplin, J.R., 2011. Void fraction measurements and scale effects in breaking waves in freshwater and seawater. *Coast. Eng.* 58, 417–428.
- Bogaert, H., Léonard, S., Brosset, L., Kaminski, M.L., 2010. Sloshing and scaling: results from the sloshel project. In: *Int. Ocean Polar Eng. Conf.*, 20th, 20–25 June. International Society of Offshore and Polar Engineers, Beijing, China.
- Bredmose, H., Peregrine, D.H., Bullock, G.N., 2009. Violent breaking wave impacts. Part 2. Modelling the effect of air. *J. Fluid Mech.* 641, 389–430.
- Bullock, G.N., Murton, G.J., 1989. Performance of a wedge-type absorbing wave maker. *J. Waterw. Port, Coast. Ocean Eng.* 115 (1) (ASCE).
- Bullock, G.N., Crawford, A.R., Hewson, P.J., Walkden, M.J.A., Bird, P.A.D., 2001. The influence of air and scale on wave impact pressures. *Coast. Eng.* 42 (4), 291–312.
- Bullock, G.N., Obhari, C., Peregrine, D.H., Bredmose, H., 2007. Violent breaking wave impacts. Part 1: results from large-scale regular wave tests on vertical and sloping walls. *Coast. Eng.* 54, 602–617.
- Chan, E.S., Melville, W.M., 1988. Deep-water plunging wave pressures on a vertical plan wall. *Proc. Roy. Soc. A* 417, 95–131.
- Crowe, A.T., Davidson, M.J., Nokes, R.L., 2016. Velocity measurements in inclined negatively buoyant jets. *Environ. Fluid Mech.* 16 (3), 503–520.
- Cuomo, G., Allsop, W., Bruce, T., Pearson, J., 2010a. Breaking wave loads at vertical seawalls and breakwaters. *Coast. Eng.* 57, 424–439.
- Cuomo, G., Piscopia, R., Allsop, W., 2010b. Evaluation of wave impact loads on caisson breakwaters based on joint probability of impact maxima and rise times. *Coast. Eng.* 58 (1), 9–27.
- Davey, T., Bruce, T., Allsop, W., 2008. Getting more from physical modelling – measuring extreme responses using importance sampling. In: *Proceedings of the International Conference on Coastal Engineering*, Hamburg.
- De Rouville, A., Besson, P., Petry, P., 1938. Etat actuel des études internationales sur les efforts dus aux lames. *Ann. Ponts Chaussées* 108 (11), 5–113.
- Denny, D.F., 1951. Further experiments on wave pressure. *J. ICE* 35 (4), 330–345.
- Dias, F., Ghidaglia, J.M., 2018. Slamming: recent progress in the evaluation of impact pressures. *Annu. Rev. Fluid Mech.* 50, 243–273. <https://doi.org/10.1146/annurev-fluid-010816-060121>.
- Duong, T.T., Jung, K.H., Lee, G.N., Kim, D.S., Suh, S.B., Kim, M.S., 2019. Experimental study on wave impact under deck due to regular waves in journal of coastal research, special issue No. 91. In: *PROCEEDINGS of the 3rd INTERNATIONAL WATER SAFETY SYMPOSIUM IWSS 2018 (SUMMER 2019)*, pp. 81–85. <https://www.jstor.org/stable/26852482>.
- EurOtop, 2018. In: Van der Meer, J.W., Allsop, N.W.H., Bruce, T., De Rouck, J., Kortenhaus, A., Pullen, T., Schüttrumpf, H., Troch, P., Zanuttigh, B. (Eds.), *Manual on Wave Overtopping of Sea Defences and Related Structures. An Overtopping Manual Largely Based on European Research, but for Worldwide Application*. www.overtopping-manual.com.
- Faltinsen, 1974. A non-linear theory of sloshing in rectangular tanks. *J. Ship Res.* 18 (4), 224–241.
- Führbötter, A., 1987. Model and prototype tests for wave impact and run-up on a uniform 1:4 slope. *Coast. Eng.* 10, 49–84.
- Grue, J., Kolaas, J., 2017. Experimental particle paths and drift velocity in steep waves at finite water depth. *J. Fluid Mech.* 810 (R1), 1–10.
- Guedes Soares, C., Pascoal, R., AntSo, E.M., Voogt, A.J., Buchner, B., 2004. An approach to calculate the probability of wave impact on an FPSO bow. In: *Proceedings of the 23rd International Conference on Offshore Mechanics and Arctic Engineering*. ASME, New York paper OMAE2004-51575.
- Ha, Y.-J., Kim, K.-H., Nam, B.W., Hong, S.Y., 2020. Experimental investigation for characteristics of wave impact loads on a vertical cylinder in breaking waves. *Ocean Eng.*, 107470 <https://doi.org/10.1016/j.oceaneng.2020.107470>.
- Hattori, M., Arami, A., Yui, T., 1994. Wave impact pressure on vertical walls under breaking waves of different types. *Coast. Eng.* 22, 79–114.
- Hodgson, T., Barltrop, N.D.P., 2004. Structural response of bow type structures to impact by steep fronted waves and resulting structural design. In: *Proceedings of OMAE Speciality Symposium on Integrity of FPSO Systems*, OMAE-FPSO'04-0064, Houston.
- Hofland, B., Kaminski, M.L., Wolters, G., 2010. Large scale wave impacts on a vertical wall. In: *Proceedings of 32nd International Conference on Coastal Engineering*, Shanghai.
- Hull, P., Muller, G., 2002. An investigation of breaker heights, shapes and pressures. *Ocean Eng.* 29, 59–79.
- Hunt-Raby, A.C., Borthwick, A.G.L., Stansby, P.K., Taylor, P.H., 2011. Experimental measurement of focused wave group and solitary wave overtopping. *J. Hydraul. Res.* 49 (4), 450–464.
- Kim, S.-Y., Kim, K.-K., Kim, Y., 2015. Comparative study on pressure sensors for sloshing experiment. *Ocean Eng.* 94, 199–212.
- Kimmoun, O., Ratouis, A., Brosset, L., 2010. Sloshing and scaling: experimental study in a wave canal at two different scales. In: *Int. Ocean Polar Eng. Conf.*, 20th, 20–25 June, Beijing, China.
- Kirkgoz, M.S., 1990. An experimental investigation of a vertical wall response to breaking wave impact. *Ocean Eng.* 17 (4), 379–391.
- Kirkgoz, M.S., 1991. Impact pressure of breaking waves on vertical and sloping walls 18 (1/2), 45–59.
- Kirkgoz, M.S., 1995. Breaking wave impact on vertical and sloping coastal structures. *Ocean Eng.* 22 (1), 35–48.
- Kortenhaus, A., Oumeraci, H., Kohlhase, S., Klammer, P., 1994. Wave induced uplift loading of caisson breakwaters. In: *Proceedings International Conference Coastal Engineering*, ASCE, Kobe, Japan, vol. 24, pp. 1298–1311. Part 2.
- Kortenhaus, A., 1997. Statistics of impact and no impact waves. *MAST III/PROVERBS MAS3-CT95-0041 Discussion Note 1–13*.
- Lubin, P., Kimmoun, O., Véron, F., Glockner, S., 2019. Discussion on instabilities in breaking waves: vortices, air-entrainment and droplet generation. *Eur. J. Mech. B Fluid* 73, 144–156. <https://doi.org/10.1016/j.euromechflu.2018.05.006>.
- Lugni, C., Brocchini, M., Faltinsen, O.M., 2010. Evolution of the air cavity during a depressurized wave impact. II. The dynamic field. *Phys. Fluids* 22, 056102. <https://doi.org/10.1063/1.3409491>.
- Ma, Z.H., Causon, D.M., Qian, I., Mingham, C.G., Mai, T., Greaves, D., Raby, A., 2016. Pure and aerated water entry of a flat plate. *Phys. Fluids* 28 (1). <https://doi.org/10.1063/1.4940043>.
- Mai, T., 2017. On the Role of Aeration, Elasticity and Wave-Structure Interaction on Hydrodynamic Impact Loading. PhD thesis at Plymouth University. <http://hdl.handle.net/10026.1/9884>.
- Mai, T., Mai, C., Raby, A., Greaves, D.M., 2020. Hydroelasticity effects on water-structure impacts. *Exp. Fluid* 61, 191. <https://doi.org/10.1007/s00348-020-03024-3>.
- Marzeddu, A., Oliveira, T.C., Gironella, F.X., Sanchez-Arcilla, A., 2017. Variability of wave impact pressures on vertical breakwaters. *J. Hydraul. Res.* <https://doi.org/10.1080/00221686.2017.1312576>.
- McConnell, K., Kortenhaus, A., 1996. Analysis of pressure measurements from hydraulic model tests and prototype measurements. In: *Proc. Task 1 Belfast Workshop, PROVERBS Project*. Leichtweiss Institut, Technical University of Braunschweig, Braunschweig, Germany. MAST III/PROVERBS.
- Minnaert, M., 1933. On musical air bubbles and the sounds of running water. *Philos. Mag.* A 16, 235–248.
- Mogridge, G.R., Jamieson, W.W., 1980. Wave impact pressures on composite breakwaters. In: *Proceedings of the 17th International Conference on Coastal Engineering (Sydney)*. <https://doi.org/10.9753/icce.v17.%25p>.
- Na, B., Kuang-An, C., Ho-Joon, L., 2020. Flow kinematics and air entrainment under laboratory spilling breaking waves. *J. Fluid Mech.* 882.

- Nikora, V., Nokes, R., Veale, W., Davidson, M., Jirka, G.H., 2007. Large-scale turbulent structure of uniform shallow free-surface flows. *Environ. Fluid Mech.* 7 (2), 159–172.
- Nokes, R., 2021. System Theory and Design. Streams Version 3.03.
- Oumeraci, H., 1994. Review and analysis of vertical breakwater failures – lessons learned. *Coast. Eng.* 22, 3–29.
- Oumeraci, H., Kortenhaus, A., 1997. Wave impact loading tentative formulae and suggestions for the development of final formulae. MAST III/PROVERBS MAS3-CT95-0041 Discussion note 1–15.
- Oumeraci, H., Kortenhaus, A., Allsop, W., de Groot, M., et al., 2001. Probabilistic Design Tools for Vertical Breakwaters. A.A. Balkema Publishers, Lisse.
- Peregrine, H., 2003. Water-wave impact on walls. *Annu. Rev. Fluid Mech.* 35, 23–43.
- Qiao, J.D., Delavan, S.K., Nokes, R.I., Plew, D.R., 2016. Flow structure and turbulence characteristics downstream of a spanwise suspended linear array. *Environ. Fluid Mech.* 16 (5), 1021–1041.
- Richert, G., 1968. Experimental investigation of shock pressures against breakwaters. Proc. 11th Conf. Coastal Eng. ASCE 1, 954–973.
- Schmidt, R., Oumeraci, H., Partensky, H.-W., 1992. Impact loads induced by plunging breakers on vertical structures. Proc. 23rd Conf. Coastal Eng. ASCE 1545–1558.
- Song, Y.K., Chang, K.-A., Ryu, Y., Kwon, S.H., 2013. Experimental study on flow kinematics and impact pressure in liquid sloshing. *Exp. Fluid* 54, 1592.
- Stagonas, D., Marzeddu, A., Cobos, F.X.G.I., Conejo, A.S.-A., Muller, G., 2016. Measuring wave impact induced pressures with a pressure mapping system. *Coast. Eng.* 112, 44–56.
- Stevenson, T., 1886. The Design and Construction of Harbours, a Treatise on Maritime Engineering, 3rd e. A.C. Black, Ltd, Edinburgh.
- van den Bremer, T., Whittaker, C.N., Calvert, R., Raby, A.C., Taylor, P.H., 2019. Experimental study of particle trajectories below deep-water surface gravity wave groups. *J. Fluid Mech.* 879.
- van Meerkerk, M., Poelma, C., Hofland, B., Westerweel, J., 2021. Gas flow dynamics over a plunging breaking wave prior to impact on a vertical wall. *Eur. J. Mech. B Fluid.* <https://doi.org/10.1016/j.euromechflu.2021.09.008>.
- Verhagen, J., 1967. The impact of a flat plate on a water surface. *J. Ship Res.* 11, 211–223.
- Vyzikas, T., Stagonas, D., Buldakov, E., Greaves, D., 2018. The evolution of free and bound waves during dispersive focusing in a numerical and physical flume. *Coast. Eng.* 132, 95–109.
- Walkden, M.J.A., Hewson, P.J., Bullock, G.N., 1996. Wave impulse prediction for caisson design. Proc. Intl. Conf. Coastal Eng. 3, 2584–2597.
- Walkden, M.J.A., Bruce, T.B., 1999. Scatter in wave load impulse maxima: a review. Proceedings of Coastal Structures '99, 439–444.
- Wang, C.Y., Teng, J.T., Huang, G.P.G., 2011. Numerical simulation of sloshing motion inside a two dimensional rectangular tank by level set method. *Int. J. Numer. Methods Heat Fluid Flow* 21 (1), 5–31.
- Whittaker, C., Raby, A.C., Fitzgerald, C., Taylor, P.H., 2016. The average shape of large waves in the coastal zone. *Coast. Eng.* 114, 253–264.
- Whittaker, C.N., Fitzgerald, C.J., Raby, A.C., Taylor, P.H., Orszaghova, J., Borthwick, A. G.L., 2017. Optimisation of focused wave group runup on a plane beach. *Coast. Eng.* 121, 44–55.
- Witte, H.H., 1991. Wave impact loading on a vertical wall with respect to structure response. In: Proceedings of 1st Workshop on Topic 2: Wave Impact Loading of Vertical Structures MAST G6-S, Hannover, June 1991.
- Yung, T.W., Ding, J., He, H., Sandstrom, R., 2009. LNG sloshing: characteristics and scaling laws. In: The Nineteenth International Offshore and Polar Engineering Conference, Osaka, Japan, pp. pp21–26.
- Zhu, L., 1995. Structural Response of Ship Plates in Slamming-Drop Test Results and Analysis. University of Glasgow, Department of Naval Architecture and Ocean Engineering-Reports-NAOE.